Research Article

Hebah A. Sindi, Ragaa A. Hamouda*, Nuha M. Alhazmi, and Marwa S. Abdel-Hamid

Functionalized gold nanoparticles coated with bacterial alginate and their antibacterial and anticancer activities

https://doi.org/10.1515/gps-2023-0170
received September 05, 2023; accepted January 2, 2024

Abstract: Gold nanoparticles (Au-NPs) have several uses for nanobiotechnologists because of their beneficial biomedical properties. Alginates have various biomedical and industrial applications. The aim of this study is to extract alginate from *Azotobacter chroococcum*, synthesize chemical Au-NPs (Ch/Au-NPs), and load the NPs with the extracted alginate to form *Azotobacter* alginate gold nanocomposites (Azto/Alg-Au-NCMs). The Ch/Au-NPs and Azto/Alg-Au-NCMs were characterized by UV-spectroscopy, Fourier-transform infrared (FT-IR) spectroscopy, energy-dispersive spectroscopy (EDS), X-ray diffraction (XRD), thermogravimetric analysis (TGA), zeta potential, and transmission electron microscopy (TEM). The anticancer activities were determined using the breast cancer cell line MCF-7, human lung cancer cell line H1299, and Vero cell line. The results obtained by UV-spectroscopy exhibited a surface plasmon resonance that was clearly noticeable at 530 nm, and the EDS analysis proved that gold was present in percentages of 50.11 and 28.08 in the Ch/Au-NPs and Azto/Alg-Au-NCMs, respectively. There were several similarities between the alginic acid and the alginate extracted from *A. chroococcum*, and small modifications were proved by FT-IR spectroscopy. Negative charges were shown by the zeta potential. Crystalline and cubic NPs were shown by XRD analysis and TEM. TGA demonstrated the purity of the Ch/Au-NPs and the existence of organic compounds in the Azto/Alg-Au-NCMs. Both the Ch/Au-NPs and Azto/Alg-Au-NCMs had antibacterial activities against *Staphylococcus aureus* ATCC 25923, *Proteus mirabilis*, *Enterobacter* sp., and *Pseudomonas aeruginosa* and possessed anticancer activities against MCF-7 and H1299.

Keywords: *Azotobacter chroococcum*, alginate, gold nanoparticles, cancer cell line, bacteria

1 Introduction

A major health challenge and cause of death globally continues to be cancer. The severity of this disease was highlighted by the estimated 19.3 million new cases and 10 million fatalities from it that were recorded in 2020 [1]. To develop novel treatment approaches, it is crucial to get a deeper understanding of the molecular mechanisms involved in both the onset and progression of cancer. The Vero cell line, which is derived from the kidney of the African green monkey, as well as the breast cancer cell line MCF7 and the non-small-cell lung cancer cell line H1299, are important lines for investigating various cancers. Millions of women around the world are affected by breast cancer, which is a severe health issue [2].

The increase in drug resistance in bacterial pathogens poses a significant obstacle to the effectiveness of antibiotics. This increase in the bacterial resistance to drugs presents a substantial challenge to health around the world. These bacteria can resist the effects of one or multiple antibiotics, leading to infections that are more difficult to manage and heightening the probability of serious sickness or fatalities. Bacteria and fungi are becoming increasingly resistant to antimicrobial medications, and it is estimated that more than 33,000 people die each year from resistant germs in Europe alone. Antimicrobial resistance has been named one of the top ten health hazards facing the global population by the World Health Organization [3,4].

* **Corresponding author: Ragaa A. Hamouda**, Department of Biology, Collage of Sciences and Arts Khulais, University of Jeddah, Jeddah 21959, Saudi Arabia; Microbial Biotechnology Department, Genetic Engineering and Biotechnology Research Institute, University of Sadat City, Sadat City 32897, Egypt, e-mail: ragaahom@yahoo.com, hamouda@gebri.usc.edu.eg, rahamouda@uj.edu.sa
Hebah A. Sindi: Department of Biological Sciences, College of Science, University of Jeddah, Jeddah 21589, Saudi Arabia, e-mail: Sindi@uj.edu.sa
Nuha M. Alhazmi: Department of Biological Sciences, College of Science, University of Jeddah, Jeddah 21589, Saudi Arabia, e-mail: nmalhazmi@uj.edu.sa
Marwa S. Abdel-Hamid: Microbial Biotechnology Department, Genetic Engineering and Biotechnology Research Institute, University of Sadat City, Sadat City 32897, Egypt, e-mail: marwa.salah@gebri.usc.edu.eg
ORCID: Ragaa A. Hamouda 0000-0002-4589-6272; Hebah A. Sindi 0000-0002-3759-0484; Nuha M. Alhazmi 0000-0001-7294-1510; Marwa S. Abdel-Hamid 0000-0003-1677-8055

Many studies have been conducted to look for alternative natural substances that can eliminate harmful bacteria, such as bio-fabricated nanoparticles (NPs) [5]. Alginate, a naturally occurring biopolymer, is mostly derived from brown algae (of the class Phaeophyceae) and specific bacterial species, such as *Azotobacter* and *Pseudomonas* [6]. This linear polysaccharide is made up of 1,4 units of -D-mannuronic acid (M) and -L-guluronic acid (G). In certain circumstances, it has the capacity to change into a substance that resembles gel. Owing to its special qualities, such as its capacity for gel formation, biocompatibility, and biodegradability, alginate has a wide range of applications in various industries. It is frequently employed in the food industry as a gelling, stabilizing, and thickening agent, as well as in the creation of edible films and coatings. Alginate has also acquired significance in the biomedical field because of its unique qualities such as biocompatibility, biodegradability, gel-forming ability, high absorbency, hemostatic capabilities, and controlled drug release ability [7,8]. These qualities have made alginate an invaluable material for uses such as cell encapsulation, tissue engineering, drug delivery systems, and wound healing. Its biocompatibility and hydrogel-forming ability make it an ideal material for a variety of medical applications, and its biodegradability ensures that it can be safely used in implantable devices and drug delivery systems without causing long-term harm [9].

A free-living, nitrogen-fixing bacterial genus called *Azotobacter* has been investigated for its possible contribution to the production of alginate. The bacterial production of alginate-like polymers was initially found in the opportunistic pathogen *Pseudomonas aeruginosa* and the soil bacterium *Azotobacter vinelandii*. The synthesis of alginates was then studied in *Azotobacter chroococcum* [10,11]. Compared with conventional seaweed-derived alginates, the alginate produced by *Azotobacter* has many benefits, including a more uniform quality, simpler purification procedures, and the potential for alteration of the alginate's composition. *Azotobacter*'s alginate has been investigated for its potential in a number of uses, including tissue engineering scaffolds, drug delivery systems, and wound dressings. In the pharmaceutical industry, alginates and alginic acid are frequently used in highly pure forms; the former is used as a stabilizer in solutions and dispersions of solid substances, and the latter is used as a binder and disintegrating agent in tablets [12].

In recent years, gold nanoparticles (Au-NPs) have sparked considerable attention owing to their potential applications in the treatment of cancer and drug-resistant microorganisms. Faraday published the first scientific paper on Au-NPs in 1857, attributing their red color to their colloidal origin and outlining their light-scattering qualities [13]. They may be created to have certain specific qualities. The stability, mobility, compatibility, and other characteristics of Au-NPs are significantly influenced by their size and shape, which should be optimized for specific biomedical applications [9,14–18]. One of the most impressive qualities of Au-NPs is their ability to convert light into heat when exposed to laser light. This characteristic is important because it can be used to create nanophotothermal vectors that can kill bacteria at the molecular level; by destroying bacterial cell walls and preventing bacterial development, they can function as antimicrobial agents on their own [19,20]. The NPs probably cause bacterial cell membrane disruption, impede bacterial enzyme function, and stimulate the creation of reactive oxygen species (ROS) that cause oxidative stress and damage to the bacterial cells [21].

Au-NPs are becoming more and more significant in a variety of biological and high-tech applications [22]. Biomolecules and drug-functionalized Au-NPs are efficiently used to treat various cancers and other diseases [23]. Bansal et al. [24] summarized the roles of Au-NPs in biomedical applications, such as curing rheumatic diseases, treating mental disorders, using for dental restorations, and improving immunity.

The combination of Au-NPs with sodium alginate increases the latter's antioxidant activity [25]. An alginate coating of Au-NPs can make it easier for nanocarriers to pass through cell membranes, improving drug delivery to tumor cells [26]. Au-NPs and cisplatin can be co-loaded into alginate, forming a compound called the ACA nanocomplex, which led to a growth inhibition of 79% in CT26 colon cancers and increased the therapeutic effectiveness of conventional chemotherapy [27].

Therefore, the aims of this study are to extract extracellular alginate from *A. chroococcum*, synthesize Au-NPs by chemical methods, and load alginate into the Au-NPs to form alginate-Au nanocomposites (Alg-Au-NCMs). In addition, the obtained Au-NPs and Alg-Au-NCMs extracted from *A. chroococcum* were tested against some isolated bacteria and the breast cancer cell line MCF-7, human lung cancer cell line H1299, and Vero cell line *in vitro*.

2 Materials and methods

2.1 *Azotobacter chroococcum* MH179061 cultivation

A. chroococcum MH179061 was obtained from the Department of Microbial Biotechnology, Genetic Engineering and Biotechnology Research Institute (GEBRI), University of Sadat City [27]. It was inoculated into modified Ashby's medium [28] and incubated for 5 days at an agitation of 350 rpm, pH of 6.84 ± 0.1, and temperature of 30°C.

2.2 Extraction of alginate from *A. chroococcum* MH179061

To extract the alginates, 1 mL of 0.5 M EDTA-sodium salt and 0.5 mL of 5 M NaCl were added to a 25 mL sample of culture broth. The mixture was mixed for 5 min before being centrifuged for 30 min at 38,000 rpm and 20°C to precipitate the cells. Alginates were precipitated from the supernatant after it had been cooled down by the addition of three volumes of ice-cold isopropanol, and they were then recovered by centrifugation at 38,000 rpm for 30 min at 4°C. After being dissolved in hot water, the white precipitate was precipitated once more, centrifuged, washing, and finally dried for 24 h at 60°C [27].

2.3 Synthesis of Au-NPs (Ch/Au-NPs)

Half mM gold auric chloride salt ($HAuCl_4$), 0.017 g was dissolved in 100 mL of double distilled water with heating near boiling (95–98°C) and then 1% tri-sodium citrate solution was added drop-wise until the solution turned to black color, with continued heating the color changed to red wine color (10 v, $HAuCl_4$: 1 v, tri-sodium citrate). After waiting until the temperature reached the room temperature, the Au-NP solution was centrifuged at 3,000 rpm for 15 min. The pellet was dispersed in deionized water by vortex and subjected to centrifugation, the re-dispersion was repeated many times to obtain almost pure Ch/Au-NPs and then stored in the dark at 2–8°C until further investigations [29].

2.4 Synthesis of gold/alginate nanocomposite (Azto/Alg-Au-NCMs)

Approximately 0.25 g of extracted alginate and 0.25 g of Ch/Au-NPs were added to 100 mL of DD water, the mixture was heated at 60–80°C and continuously stirred at 600 rpm using a magnetic stirrer till the mixture turned to deep red wine. The obtained suspension was centrifuged at 15,000 rpm for 45 min, the precipitated sample was lyophilized, and then stored in a cool, dry, and dark place until their physiochemical characterizations were estimated.

2.5 Characterizations of Ch/Au-NPs and Azto/Alg-Au-NCMs

The characterization of Ch/Au-NPs and Azto/Alg-Au-NCMs by UV-Vis spectrophotometry, transmission electron microscopy (TEM) (JEOL JSM-6510/v, Tokyo, Japan), energy-dispersive spectroscopy (EDS) (JEOL JSM-6510/v, Tokyo, Japan), zeta potential analysis (Malvern Zeta size Nano-Zs90, Malvern, PA, USA), Fourier-transform infrared (FT-IR) spectrometer, Thermo Fisher Nicolet IS10, (Waltham, MA, USA), X-ray diffractometer (PANanalytical X-Pert PRO, Spectris plc, Almelo, The Netherlands), and thermogravimetric analysis (TGA).

2.6 Anticancer activities

The anticancer activities of Azto/Alg-Au-NCMs on the breast cancer cell line (MCF-7), human lung cancer cell line (H1299), and Vero cell line (obtained from National Cancer Institute Pharmacology Unit, Cairo university) were evaluated by 3-(4,5-dimethylthiazol-2-yl)-2,5-diphenyltetrazolium bromide (MTT) assay [30].

2.7 Antibacterial activities

The antibacterial activity of Ch/Au-NPs and Azto/Alg-Au-NCMs was displayed against some pathogenic bacteria, Gram-negative, *Proteus mirabilis*, *Enterobacter* sp., and *Pseudomonas aeruginosa*, as well as Gram-positive, and *Staphylococcus aureus* ATCC 25923, the bacteria obtained from Department of Microbial Biotechnology, GEBRI, University of Sadat City. All the bacterial isolates were cultured in nutrient broth at 37°C for 24 h. Approximately 50 µL of bacterial suspension (10^{-4}) was spread over Mueller-Hinton agar (Sigma-Aldrich Company). Wells were made on the agar plates and occupied with 100 µL of each Ch/Au-NPs and Azto/Alg-Au-NCMs (5 mg·mL^{-1}). After 24 h of incubation at 37°C, the clear zones were measured.

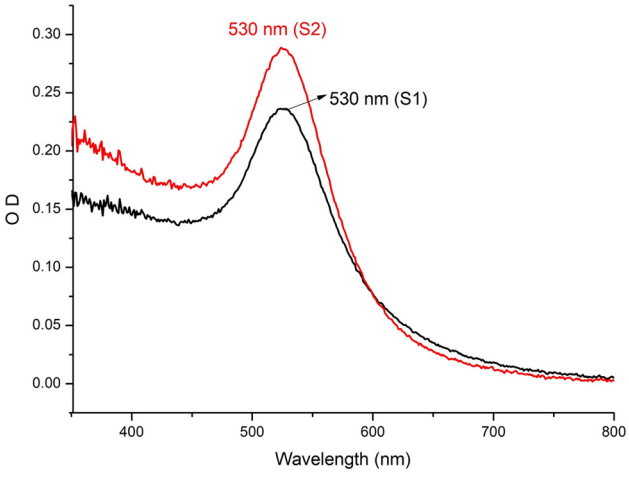

Figure 1: UV-spectrophotometer of Ch/Au-NPs (S1) and Azto/Alg-Au-NCMs (S2).

2.8 Statistical analysis

Data of the effect of Ch/Au-NPs and Azto/Alg-Au-NCMs on bacterial pathogens were presented as the mean standard error and were subjected to statistical analysis using one-way analysis of variance. The *post hoc* differences between means were tested by Tukey's multiple comparison tests. Differences at $P < 0.05$ were reflected as significant.

3 Results and discussion

3.1 UV-spectrophotometer

The presence of Au-NPs was first detected by color changes and then confirmed using a UV-spectrophotometer. The examination of the NPs benefited greatly from UV-spectrophotometry. Figure 1 shows the UV-spectrophotometry findings for Ch/Au-NPs and Azto/Alg-Au-NCMs. The results showed that the surface plasmon resonance was clearly noticeable at 530 nm for both the Ch/Au-NPs and Azto/Alg-Au-NCMs, but the optical density for the Ch/Au-NPs was 0.29 nm and for the Azto/Alg-Au-NCMs was 0.24 nm. The results agreed with those of Haiss et al. [31], who found a surface plasmon resonance of Au-NPs that had a peak of 520–580 nm and was therefore quite apparent. The surface plasmon resonance peak of Au-NPs was detected at 560 nm [32] and 550 nm [33].

3.2 FT-IR analysis of commercial alginic acid and alginate extracted from *A. chroococcum* MH179061

The FT-IR spectrum of commercial sodium alginate and alginate extracted from *A. chroococcum* MH179061 is shown in Table 1 and Figure 2. Twenty peaks appeared in the commercial sodium alginate and 23 peaks in the alginate extracted

Table 1: FT-IR analysis of commercial alginate extracted from *A. chroococcum* and alginic acid

Bacterial alginate wave (cm^{-1})	Alginic standard wave (cm^{-1})	Shift	Assignment	Ref.
3,442	3,386	−56	OH bonds	[38]
2,974	—	—	C–H stretching	[39]
2,932	2,926	−6	methylene group	[39]
2,897	—	—	C–H symmetrical stretching	[40]
2,665	—	—	N–H bond associated with amide	[41]
2,530	—	—	S–H band	[42]
2,409	—	—	OH	[43]
2,130	2,111	—	C═C bond stretching	[44]
1,922	—	—	CO bound	[45]
1,647	1,613	−34	C═O (quinonic form)	[46]
—	1,588	—	Vibrational stretching band of CO_2	[47]
1,456	—	—	Asymmetric CH_3 bending	[48]
1,409	1,422	+13	–CH deformation	[49]
1,381	—	—	CH_2 deformation	[50]
1,341	1,337	−4	CH_3 deformation	[51]
1,307	1,307	—	Proteins or CH_2	[52]
—	1,270	—	Si–CH_3	[53]
—	1,283	—	C–O–C	[54]
—	1,243	—	C–O stretching	[55]
1,162	1,175	−5	–C–O stretch	[56]
1,128	—	—	C–O stretching vibration	[57]
1,089	1,080	–9	Symmetric PO_2– vibration	[58]
1,047	1,020	−27	C═O groups	[59]
950	933	−17	OH mode	[60]
879	845	−34	C–O stretch	[61]
815	—	—	Sugar-phosphate	[62]
—	761	+	Specific to substituted aromatic ring	[63]
663	706	+43	C–S stretching modes	[64]
—	576	—	Primary alcohol skeleton bend	[65]
—	527	—	COC bending, glycosidic links/CCC ring deform	[66]

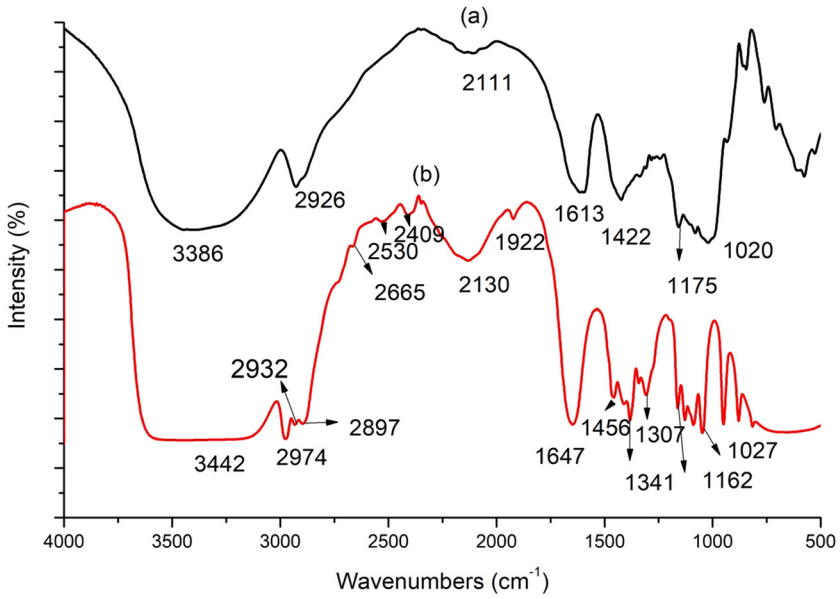

Figure 2: FT-IR analysis of commercial sodium alginic acids (a) and alginate extracted from *A. chroococcum MH179061* (b).

from *A. chroococcum* MH179061. The peaks at wavelengths of 3,442, 2,932, 2,130, 1,647, 1,049, 1,341, 1,162, 1,089, 1,047, 950, 879, and 663 cm^{-1} that were found in the alginate extracted from *A. chroococcum* MH179061 resembled the peaks that appeared for the commercial sodium alginate with some shifts. These peaks indicated the presence of functional groups such as OH bonds, the methylene group, C═C bond stretching, C═O (quinonic form), –CH deformation, CH_3 deformation, –C–O stretch, symmetric PO_2– vibration, C═O groups, OH mode, C–O stretch, and C–S stretching modes, respectively. Certain peaks were

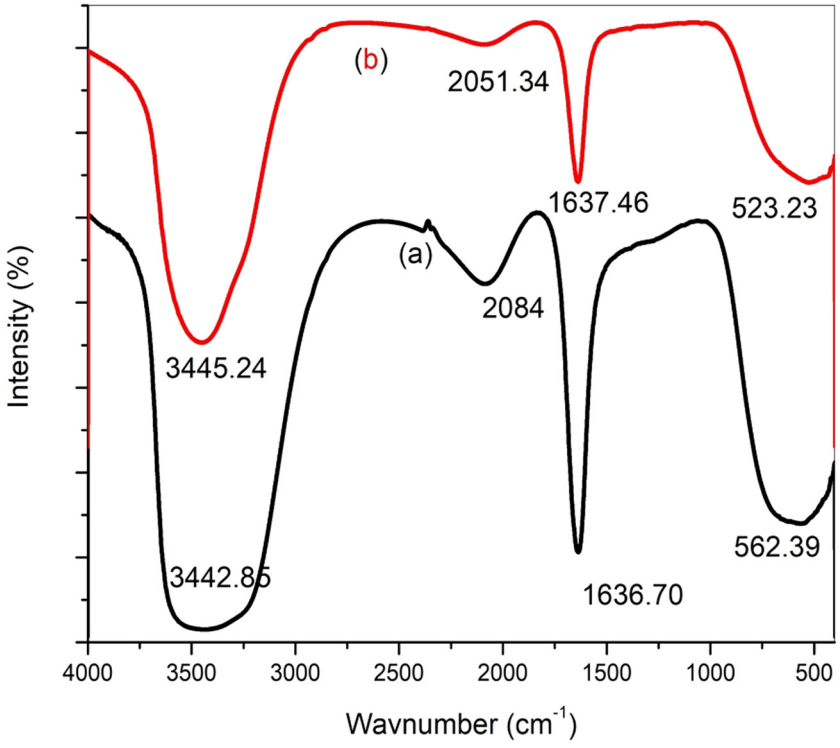

Figure 3: FT-IR analysis of Ch/Au-NPs (a) and Azto/Alg-Au-NPs (b).

found in the bacterial alginate but not in the alginate standard, such as those at the wavelengths of 2,974, 2,897, 2,665, 2,530, 2,409, 1,456, 1,381, 1,128, and 815 cm^{-1}, this may have been related to certain amino acids and proteins (enzymes) secreted by *A. chroococcum* MH179061. Some peaks that were found in the alginate standard disappeared in the bacterial alginate, such as those at the wavelengths of 1,588, 1,270, 1,283, 1,243, and 761 cm^{-1}, which suggests that some modification of the bacterial alginate compared with the commercial alginate may have been due to the sources of fabrication of the commercial alginate. Alginic acid is extracted from brown algae [34]. The alginate extracted from brown algae is different from the alginate extracted from bacteria due to the presence of *O*-acetyl groups in the bacterial alginate [35] and the presence of the alginate (polysaccharide) in the algal cell wall [36]. However, an exopolysaccharide is secreted by some types of bacteria, such as *Azotobacter* and *Pseudomonas*. The alginates produced by the two bacteria have several similarities but also are somewhat different [37].

FT-IR spectra recorded for both the Ch/Au-NPs and Azto/Alg-Au-NPs are shown in Figure 3. The absorption bands of the Ch/Au-NPs are seen at wavelengths of 3,442.85, 2,084,

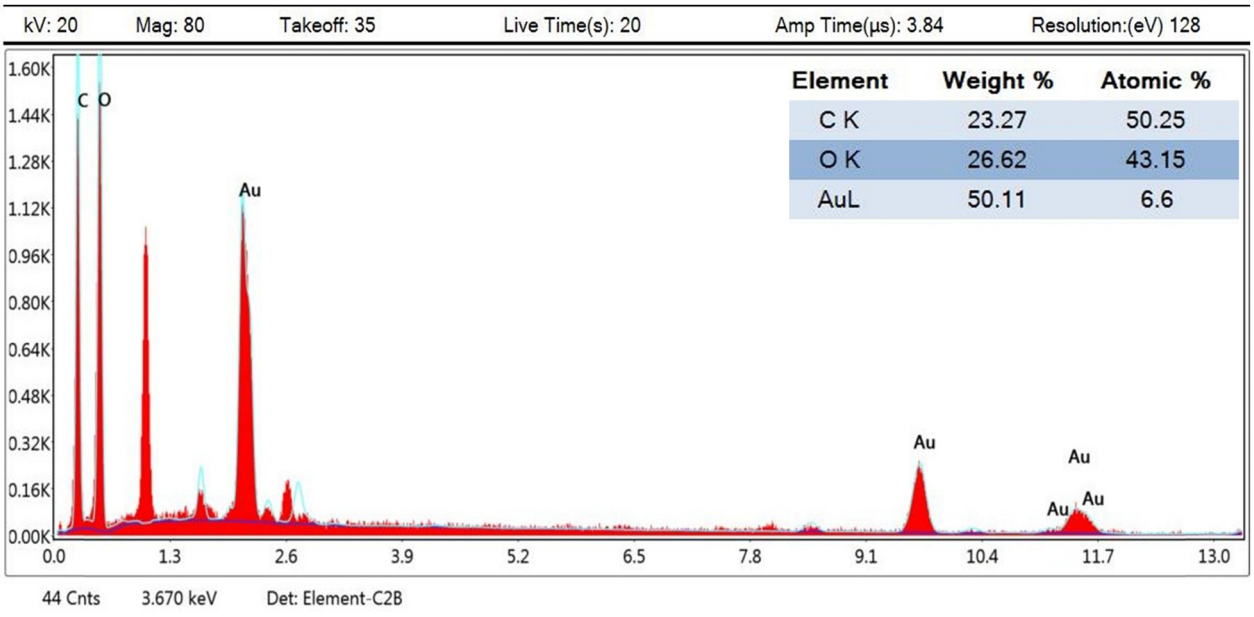

(a)

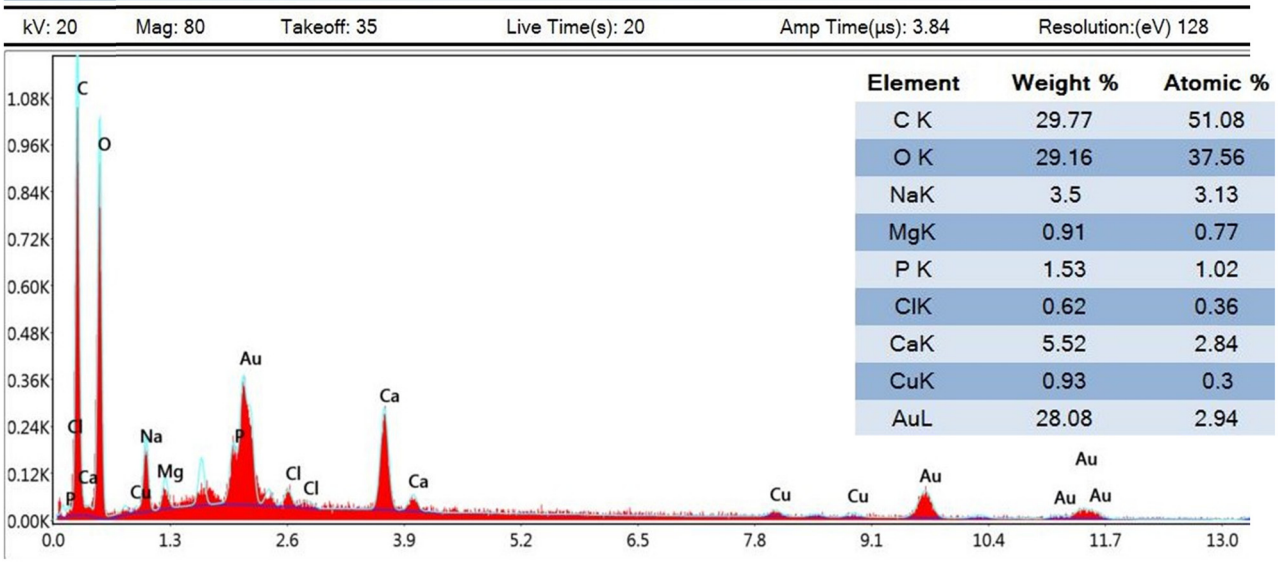

(b)

Figure 4: EDX spectrum analysis and weight% of Ch/Au-NPs (a) and Azto/Alg-Au-NPs (b).

1,636, and 562 cm^{-1}, with small differences seen in the bands of Azto/Alg-Au-NPs at wavelengths of 3,445, 2,091, 1,637, and 523 cm^{-1}. The bands at 3,442 and 3,445 cm^{-1} were attributed to the OH group and found in Au-NPs according to Hadi and Yas [67]. The band at 2,048 cm^{-1} was attributed to CO [68] and at 2,091 cm^{-1} to C–H band stretching [69]. The sharp peaks at 1,636 and 1,637 cm^{-1} were attributed to the amide group [70]. Broad bands at 562 and 523 cm^{-1} were attributed to metal oxide [71].

3.3 Energy-dispersive X-ray (EDX) analysis

EDX analysis was used to indicate the presence of Au-NPs. Figure 4 shows that the weight of gold in the Ch/Au-NPs was 50.11% at different kilo-electron volts (keV), with the major peak located at approximately 2 keV, and that the weight percentage was decreased to 28.08% in the Azto/Alg-Au-NCMs due to the presence of the alginate that was capping the Au-NPs. Some other elements also appeared, such as C, O, Na, Mg, P, Cl, Ca, and Cu, at weights of 29.77%, 29.16%, 3.5%, 0.91%, 1.53%, 0.65%, 5.52%, and 0.93%, respectively. The presence of metals such as Mg^{++}, P, Cl^{-}, and Ca^{++} may have been related to the medium used to produce the alginate from the bacteria. The absorption metallic gold located at 2 keV demonstrated the presence of Au-NPs [72].

3.4 Zeta potential

The zeta potential measures the number of electric charges on a NP's surface. Due to electrostatic repulsions, which are determined by the zeta potential, NPs are typically regarded as stable if the zeta potential is more positive than +30 mV or more negative than –30 mV [73]. Figure 5 shows the zeta potentials of the Ch/Au-NPs and Azto/Alg-Au-NPs. The zeta potential of the Ch/Au-NPs was a negative charge in the range of –30 mV, and the zeta potential of the Azto/Alg-Au-NPs was also a negative charge of –36 mV. The

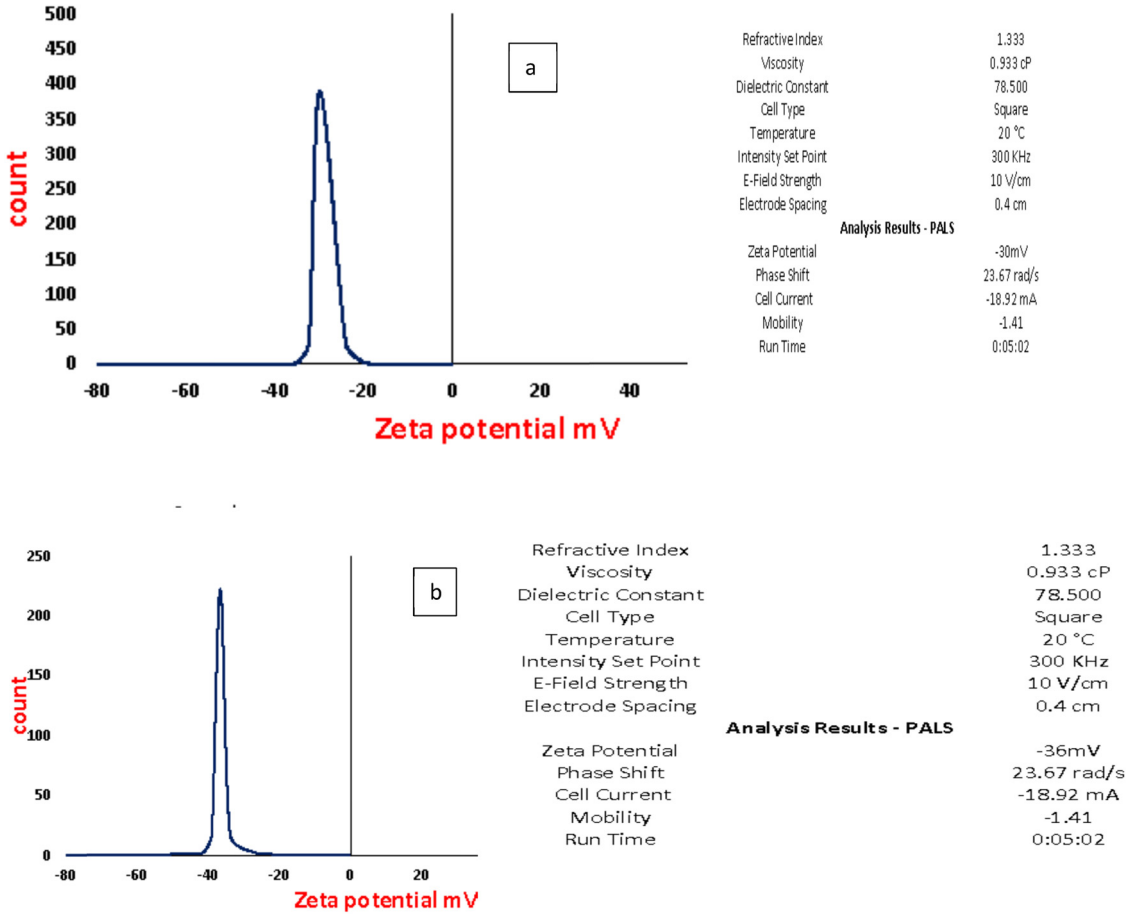

Figure 5: Zeta potential of Azto/Alg-Au-NPs (a) and Ch/Au-NPs (b).

Azto/Alg-Au-NPs had charges that were more negative than those of the Ch/Au-NPs; this was due to the adsorption by the alginate on the surface of the Ch/Au-NPs and the enhanced stability of the Azto/Alg-Au-NPs. The zeta potential of the Au-NPs prepared in pure water was –10.80 mV, and the zeta potentials of the Au-NPs prepared in alginate ranged from –40.60 to –55.17 mV. As a result, the electrostatic and steric repulsion of the "COO" groups of alginate chains was stronger than that of the Au-NPs synthesized in pure water [74,75]. The zeta potential of the Au-NPs dispersed in different concentrations of alginate ranged from −40.60 to −55.17 mV. Alginate can be used to stabilize Au-NPs and reduce the rate at which large Au-NPs precipitate [76]. The negatively charged surface of polyvinyl pyrrolidone-capped Au-NPs prevents flocculation and, hence, stabilizes the colloids through electrostatic repulsion and steric action [77]. Citrate-Au-NPs were highly stable, with an average zeta potential of −38.7 ± 4.4 mV [78].

3.5 X-ray diffraction (XRD) analysis

Figure 6a shows the XRD patterns of chemically synthesized Au-NPs (Ch/Au-NPs). They demonstrate that the Au-NPs were crystalline and cubic in shape. The XRD diffraction patterns of Ch/Au-NPs were recorded at 2-theta as 37.374°, 43.427°, 63.098°, 75.692°, 79.702°, and 95.456°, which corresponded to lattice planes (hkl) of 111, 200, 220, 311, 222, and 400. Figure 6b denotes the XRD patterns of the nanocomposites of alginate extracted from *A. chroococcum* MH179061 and the chemical synthesis of the Au-NPs (Azto/Alg-Au-NPs). The results demonstrate that the Azto/Alg-Au-NPs were crystalline and cubic in shape. The XRD diffraction patterns of the Azto/Alg-Au-NPs were recorded at 38.272°, 44.485°, 64.726°, 77.760°, 81.935°, and 98.410°, which corresponded to lattice planes (hkl) of 111, 200, 220, 311, 222, and 400, respectively. There were small modifications in the peak positions between the Ch/Au-NPs and Azto/Alg-Au-NPs,

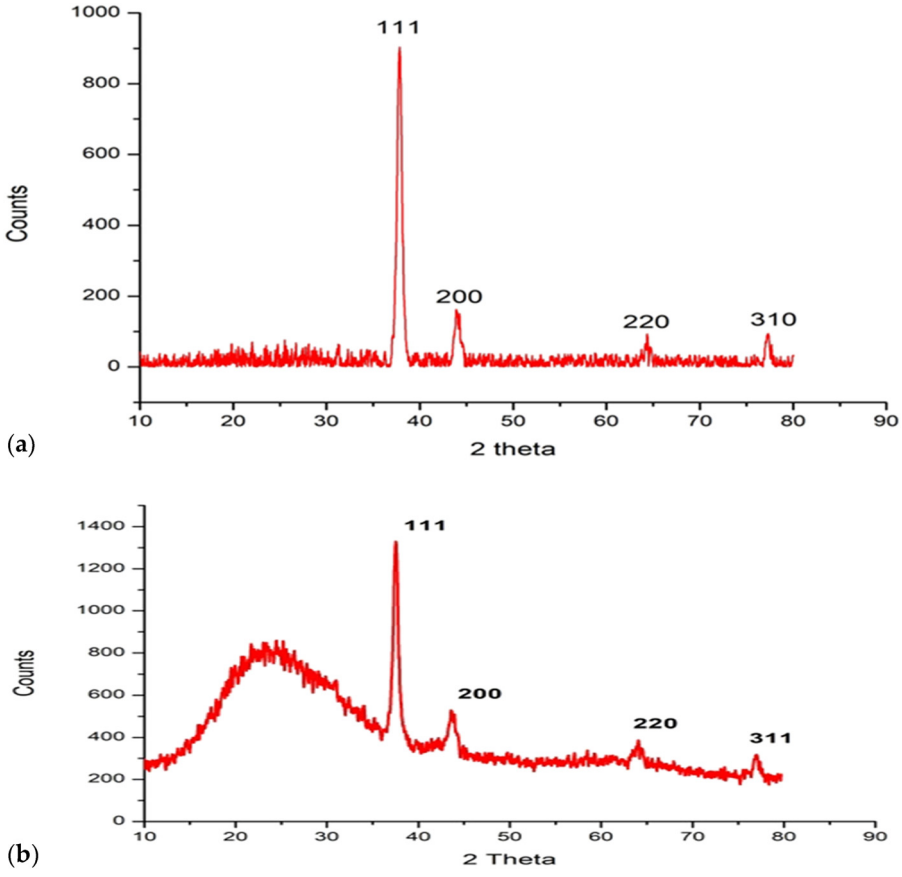

Figure 6: XRD analysis of Ch/Au-NPs (a) and Azto/Alg-Au-NCMs (b).

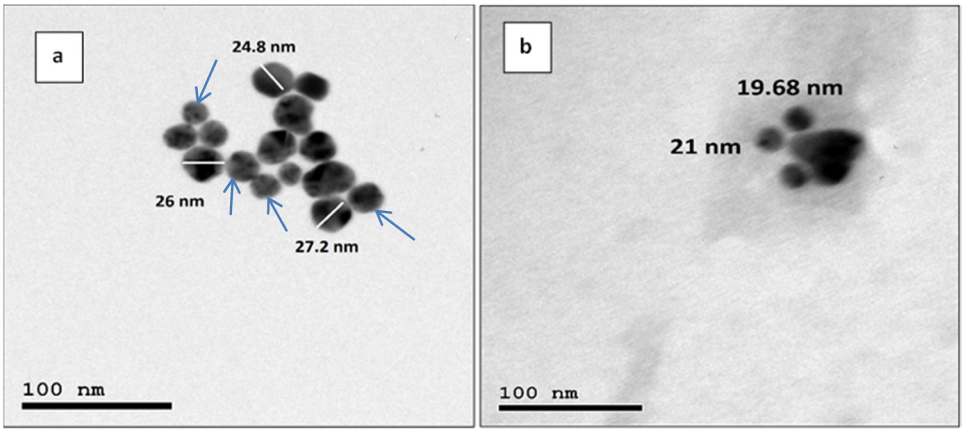

Figure 7: TEM of Azto/Alg-Au-NPs (a) and Ch/Au-NPs (b), arrows refer to alginate loaded in Au-NPs.

and this denoted the presence of the alginate that was coated on the Au-NPs. The strongest peak was at hkl 111 for both the Ch/Au-NPs and Azto/Alg-Au-NPs. There was a shift in 2-theta to a higher angle in the case of the Azto/Alg-Au-NPs, and this was due to the small size of the Azto/Alg-Au-NPs in comparison with the Ch/Au-NPs. The slight shift of the strongest peak (111) to a higher angle occurred as the particle size became smaller [79]. The obtained results were quite similar to those in the study by Bindhu and Umadevi [29], who reported diffraction peaks of biosynthesized Au-NPs at the 2-theta range of 38.21°, 44.11°, 64.81°, and 77.61°, and they were parallel to the numbers 111, 200, 220, and 311, respectively, of the Bragg reflection.

3.6 TEM images

Figure 7 shows the TEM images of the Ch/Au-NPs and Azto/Alg-Au-NPs. The images clarified the cubic geometry in terms of the shapes of the Ch/Au-NPs and Azto/Alg-Au-NCMs. The size of the Azto/Alg-Au-NCMs ranged from 24 to 27 nm and of the Ch/Au-NPs from 19.97 to 22 nm. These results demonstrated that the obtained NPs were nearly monodispersed. The shape of the Au-NPs differed according to the synthesis process. The Au-NPs synthesized by a solvothermal method using tin chloride ($SnCl_2$) as a reducing agent had a nearly spherical geometry, ranging in size from 5 to 50 nm, and had an average particle size of 15 nm [80]. Au-NP synthesis by the isopropanol extract alfalfa biomass ranged from 30 to 60 nm in diameter and had low surface energy [81]. Chemically synthesized Au-NPs synthesized by pure water were mostly spherical and more aggregated than those synthesized in the presence of alginate [76]. The average size was 15–20 nm for the Au-NPs embedded in polyethylene oxide and sodium alginate polymer [82].

3.7 TGA findings

The TGAs of the Ch/Au-NPs and Azto/Alg-Au-NPs are provided in Figure 8a and b. The Ch/Au-NPs show a one-step loss of weight, whereas the Azto/Alg-Au-NPs show a two-step loss of weight. The weight of the Azto/Alg-Au-NPs was

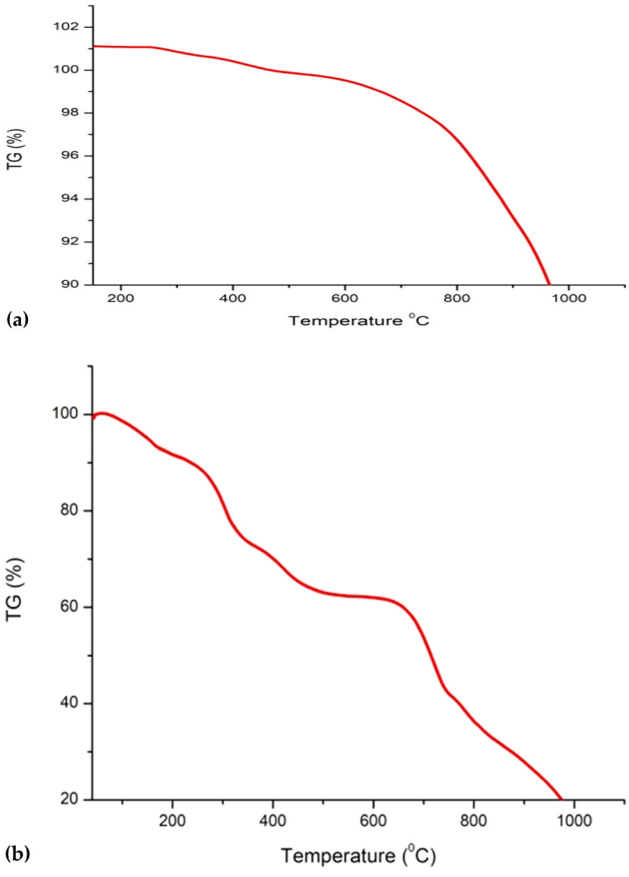

Figure 8: TGA curves of Ch/Au-NPs (a) and Azto/Alg-Au-NPs (b).

determined in an aqueous solution; it could therefore be proposed that a layered structure of alginate was formed around the surface of the gold via the OH groups and was connected to the gold, the OH groups of which were in an aqueous solution, through hydrophobic interaction. Loss of weight may be attributed to the loss of the alginate layer first, followed by the loss of the gold. Similar results were found by Tajammul Hussain et al. [83]; the first and second weight losses of the starch-capped Au-NPs in the TGA curve might be attributed to the releases of the outer and inner layers of the surfaces, respectively. TGA of pentafluorobenzenethiolate with $Au_{55}(PPh3)_{12}Cl_6$ showed a two-step weight loss, and this proved the formation of the ligand shell's composition [84]. TGA of biosynthesized Au-NPs by an apiin compound showed that the weight loss at 150°C was attributed to the water molecules extant in the apiin compound, followed by a steady weight loss until 800°C that was due to the surface desorption of bioorganic materials found with the NPs [85].

3.8 Anticancer activities

Figure 9a and b displays the anticancer activities of different concentrations of Azto/Alg-Au-NPs against the breast cancer cell line MCF-7, human lung cancer cell line H1299, and Vero cell line. The Azto/Alg-Au-NPs had good results

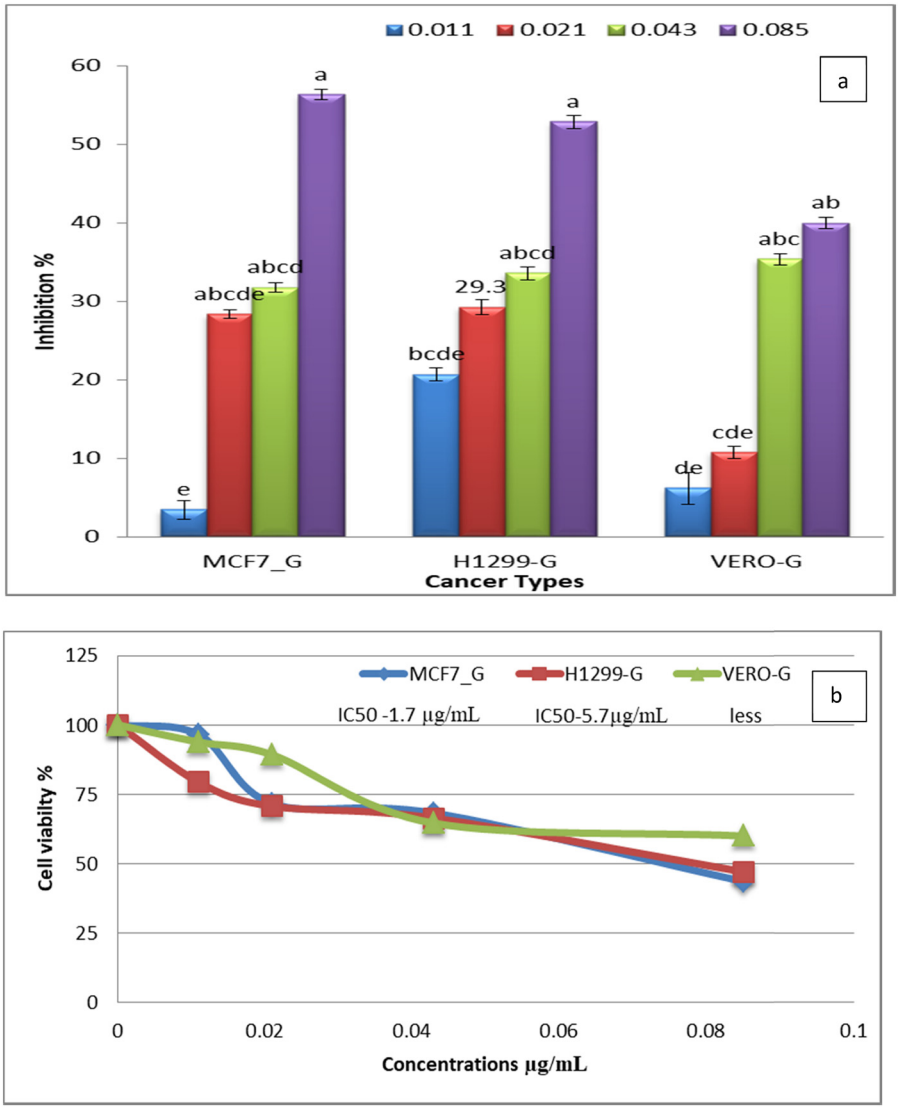

Figure 9: (a) Anticancer activities of different concentrations of Azto/Alg-Au-NPs (µg·mL^{-1}) against breast cancer cell line (MCF-7), human lung cancer cell line (H1299), and Vero cell line (different letters, denote significant values). (b) Cell viability rate of breast cancer cell line (MCF-7), human lung cancer cell line (H1299), and Vero cell line that were pre-treated with Azto/Alg-Au-NPs.

against the breast cancer cell line MCF-7 and the human lung cancer cell line H1299, which had inhibition percentages of 56.4% and 52.9% at 0.085 μg·mL^{-1} Azto/Alg-Au-NPs. A low level of inhibition was shown with the Vero cell line. Figure 9 shows the cell viability rate of the breast cancer cell line MCF-7, human lung cancer cell line H1299, and Vero cell line that were pretreated with Azto/Alg-Au-NPs. Chloroquine-Au-NP conjugates exhibited anticancer activity against MCF-7 breast cancer cells [86]. The plant-mediated Au-NPs that were 30 nm in size showed anticancer activity against MCF-7 breast cancer cells with a minimum inhibitory concentration of 2 μg·mL^{-1}; as the concentrations increased, the anticancer activity also increased [87]. Methotrexate/alginate/curcumin/Au-NPs displayed active targeting efficacy against MCF-7 cancer cells [88]. The biosynthesized Au-NPs obtained via extraction from the *Nigella arvensis* leaf had

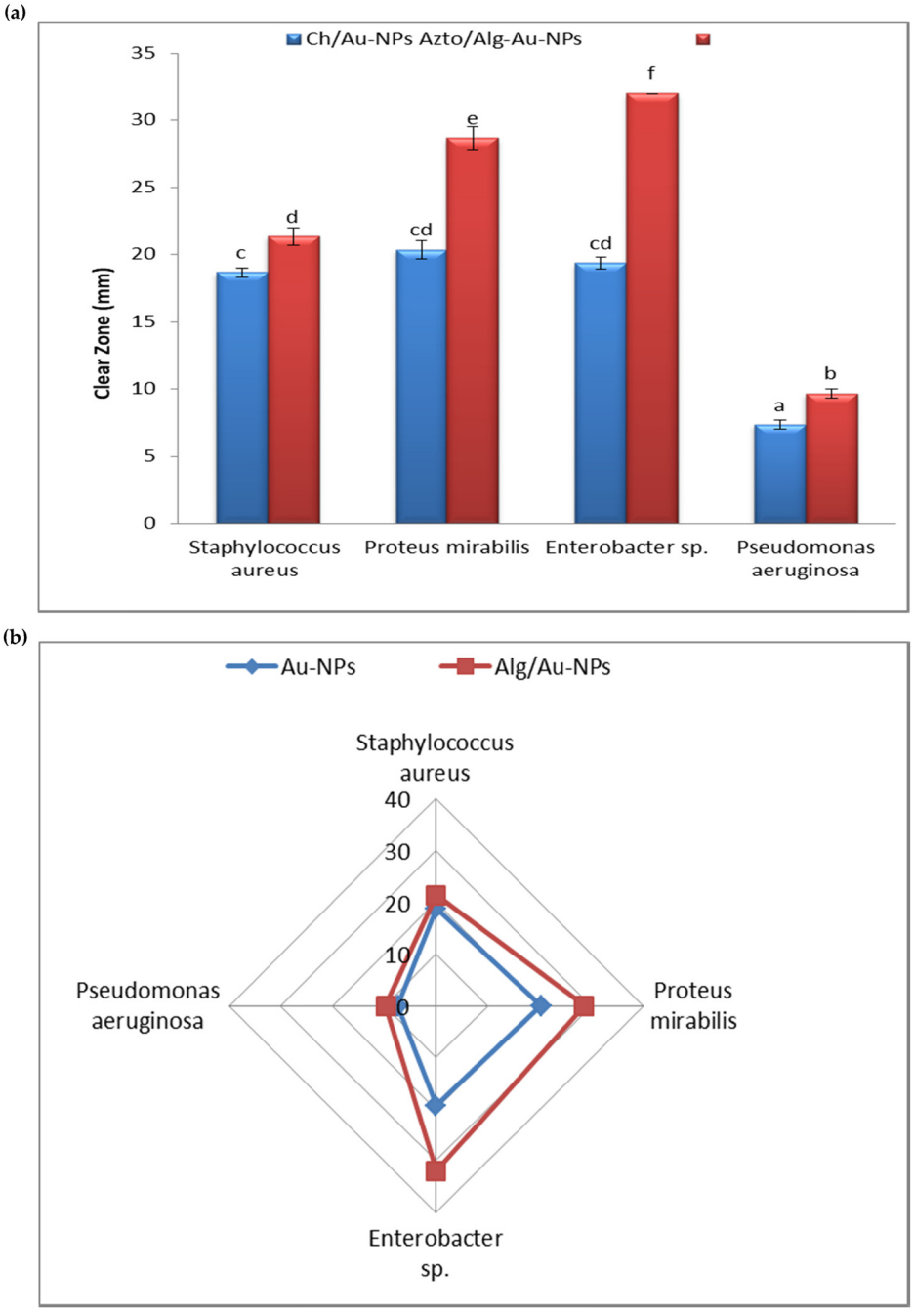

Figure 10: (a) Antibacterial activities by agar well diffusion as a model of Ch/Au-NPs and Azto/Alg-Au-NPs against bacterial isolates (different letters, denote significant values). (b) Radar analysis shows the inhibition zone (mm) of both Ch/Au-NPs and Azto/Alg-Au-NPs against bacterial isolates.

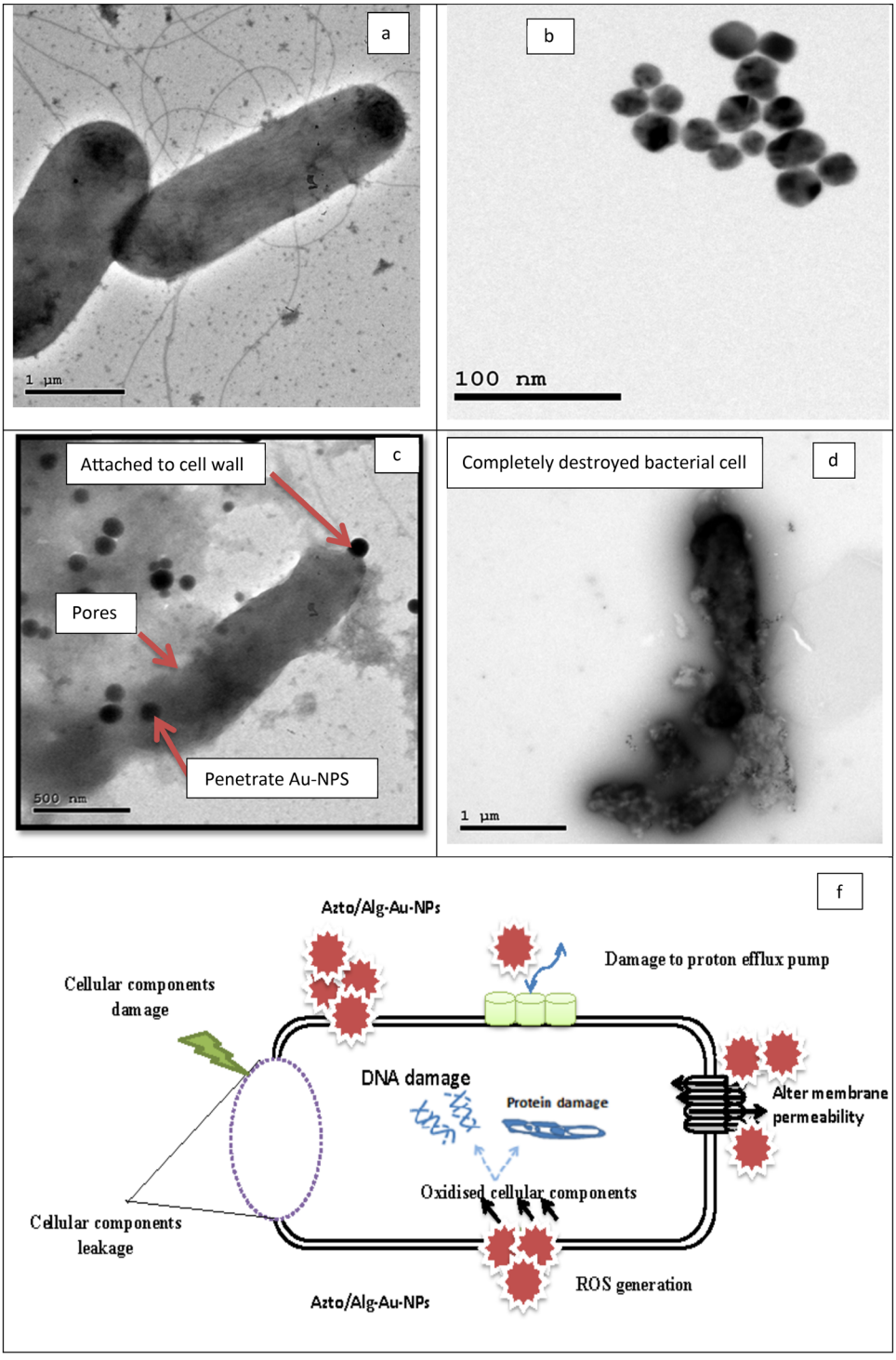

Figure 11: HR-TEM examination of *Proteus mirabilis* with treated with Azto/Alg-Au-NPs. Healthy cell (a), treated bacteria (b), TEM image of Azto/Alg-Au-NPs (c), destroyed bacteria (d), and suggested mechanism (e).

anticancer activities against H1299 and MCF-7 cancer cell lines with a half-maximal inhibitory concentration (IC50) of 10 and 25 $\mu g \cdot mL^{-1}$, respectively [89]. The IC50 of cells with silver NPs was 35.8 $\mu g \cdot mL^{-1}$ [90]. Curcumin-coated Au-NPs and their composites with chitosan/sodium were cytotoxic against the UM-UC-6 and MDA-MB 231 cell lines *in vitro* [91]. The gold/cellulose nanocomposite was cytotoxic against A549 cancer lung cells and HEL299 normal lung fibroblasts, and it also reduced the relative expression of the Raf-1 gene [92]. The inhibition percentage was lower against the Vero cell line,

and this finding agreed with the findings of Priya and Iyer [93] that various concentrations of Au-NPs were nontoxic against the Vero cell line.

3.9 Antibacterial activities

Figure 10a and b show the antibacterial activities of both the Ch/Au-NPs and Azto/Alg-Au-NPs against the bacterial isolates *Staphylococcus aureus* ATCC 25,923, *Proteus mirabilis*, *Enterobacter* sp., and *P. aeruginosa,* which were evaluated by disc diffusion methods. Both the Ch/Au-NPs and Azto/Alg-Au-NPs had significant antibacterial activities against all tested bacteria. The Azto/Alg-Au-NPs were more effective against *Enterobacter* sp. but less effective against *P. aeruginosa.* There were no significant changes in the effect of Ch/Au-NPs against *P. mirabilis* or *Enterobacter* sp. Results demonstrated that the Azto/Alg-Au-NPs had greater antibacterial activity than the Ch/Au-NPs for all tested bacteria. A gold-peptide-alginate hydrogel was shown to have antimicrobial activity against pathogenic bacteria. A gold–gold alginate polymer could be promising in a very short time, which would make it potentially helpful for industrial and biomedical applications [94]. A composite of Au-NPs/polyaniline boronic acid/sodium alginate, which had an average size of 15–20 nm and a zeta potential of −32.5 ± 1.6 mV, had antibacterial activity against seafood-associated bacterial isolates [95]. Gold nanocomposites based on polysaccharides such as alginate and chitosan possessed antibacterial activity against gram-negative *P. aeruginosa* and gram-positive *S. aureus* [96]. Curcumin-coated Au-NPs and their composites with chitosan/sodium had antibacterial activities against *S. aureus* and *E. coli* [91].

TEM images of *P. mirabilis* gram-negative bacteria when used as a control and when treated by Azto/Alg-Au-NPs are shown in Figure 11. The Au-NPs became attached to the cell membrane, penetrated the cell, made holes in the cell wall, and finally completely destroyed the cell, which affirmed the mechanisms that had been suggested in many research studies. Glycol chitosan NPs were attached to the surface of methicillin-resistant *S. aureus* cells to alter the cells' permeability, block the nutrient flow, and disrupt the cell membranes. Poly(γ-glutamic acid) NPs penetrated *Salmonella enterica* cells, forming cell wall cavities, plasmolysis, and degeneration [97]. A gold-titanium dioxide/sodium alginate composite had an antibacterial effect against *S. aureus* and *E. coli* in light conditions. The antibacterial property of the film arose from the improved production of ROS prompted by the surface plasmonic resonance of Au-NPs. The degradable and antibacterial properties reduced the composite film; this could have major potential in the food packaging industry [98]. Nanocomposites could be inexpensive and safe products when extracted from natural sources with antibacterial components [99].

4 Conclusion

The alginate produced by *A. chroococcum* is a good source for the production of Azto/Alg-Au-NCMs. The synthesis of Ch/Au-NPs and Azto/Alg-Au-NCMs was confirmed by FT-IR and EDS analysis. There were peaks that appeared in the commercial sodium alginate and the alginate extracted from bacteria with some small modifications shown on FT-IR spectroscopy. The zeta potential proved the negative charge of the Ch/Au-NPs, at –30, and of the Azto/Alg-Au-NCMs, at –36. The XRD patterns confirmed the crystalline nature of both the Ch/Au-NPs and Azto/Alg-Au-NCMs, according to the 2-theta angle and lattice planes (hkl) that appeared. The results obtained by EDX spectrum analysis denoted the percentages of gold in the Ch/Au-NPs (50.11%) and in the Azto/Alg-Au-NCMs (28.08%). TEM images proved that the Ch/Au-NPs were spherical in shape and ranged in size from 24 to 27 nm, and that the Azto/Alg-Au-NCMs were also spherical in shape and ranged in size from 19.97 to 22 nm. Both the Ch/Au-NPs and Azto/Alg-Au-NCMs possessed antibacterial activity against *S. aureus* ATCC 25923, *P. mirabilis*, *Enterobacter* sp., and *P. aeruginosa.* The Azto/Alg-Au-NCMs had anticancer effects against the breast cancer cell line MCF-7 and human lung cancer cell line, but were less effective against the Vero cell line *in vitro*.

Acknowledgements: This work was funded by the Deanship of Scientific Research (DSR), University of Jeddah, Jeddah, Saudi Arabia, under Grant No. UJ-22-DR-103. The authors, therefore, acknowledge with thanks the technical and financial support from DSR.

Funding information: This work was funded by the Deanship of Scientific Research (DSR), University of Jeddah, Jeddah, Saudi Arabia, under Grant No. UJ-22-DR-103. The authors, therefore, acknowledge with thanks the technical and financial support from DSR.

Author contributions: H.A.S.: investigation, writing, resources, and reviewing. R.A.H.: conceptualization, data analysis, validation, writing, and reviewing. N.M.A.: investigation, writing, and resources. M.S.A.: methodology, writing, and reviewing. All authors have read and agreed to the published version of the manuscript.

Conflict of interest: Authors state no conflict of interest.

Data availability statement: The datasets generated during and/or analyzed during the current study are available from the corresponding author on reasonable request.

References

[1] Sung H, Ferlay J, Siegel RL, Laversanne M, Soerjomataram I, Jemal A, et al. Global cancer statistics 2020: GLOBOCAN estimates of incidence and mortality worldwide for 36 cancers in 185 countries. CA: Cancer J Clin. 2021;71(3):209–49.

[2] Soule HD, Vazquez J, Long A, Albert S, Brennan MA. Human cell line from a pleural effusion derived from a breast carcinoma. J Natl Cancer Inst. 1973;51(5):1409–16.

[3] Molina JR, Yang P, Cassivi SD, Schild SE, Adjei AA. Non-small cell lung cancer: Epidemiology, risk factors, treatment, and survivorship. Mayo Clin Proc. 2008;83(5):584–94.

[4] Ljungberg B, Campbell SC, Choi HY, Jacqmin D, Lee JE, Weikert S, et al. The epidemiology of renal cell carcinoma. Eur Urol. 2011;60(4):615–21.

[5] Centers for Disease Control and Prevention (CDC). Antibiotic resistance threats in the United States. 2019. Retrieved from. https://www.cdc.gov/drugresistance/pdf/threats-report/2019-ar-threats-report-508.pdf.

[6] Organisation for Economic Co-operation and Development (OECD). Stemming the Superbug tide: Just a few dollars more. 2019. Retrieved from. https://www.oecd-ilibrary.org/social-issues-migration-health/stemming-the-superbug-tide_9789264307599-en.

[7] World Health Organization (WHO). Antimicrobial resistance. 2021. Retrieved from. https://www.who.int/news-room/fact-sheets/detail/antimicrobial-resistance.

[8] Alhazmi NM. Fungicidal activity of silver and silica nanoparticles against aspergillus sydowii isolated from the soil in Western Saudi Arabia. Microorganisms. 2023;11:86. doi: 10.3390/microorganisms11010086.

[9] Lee KY, Mooney DJ. Alginate: Properties and biomedical applications. Prog Polym Sci. 2012;37(1):106–26.

[10] Stender EGP, Andersen CD, Fredslund F, Holck J, Solberg A, Teze D, et al. Structural and functional aspects of mannuronic acid–specific PL6 alginate lyase from the human gut microbe bacteroides cellulosilyticus. J Biol Chem. 2019;294(47):17915–30.

[11] Qin Y, Jiang J, Zhao L, Zhang J, Wang F. Applications of alginate as a functional food ingredient. In biopolymers for food design. Cambridge, Massachusetts: Academic Press; 2018. p. 409–29. doi: 10.1016/B978-0-12-811449-0.00013-X.

[12] Varghese S, Elisseeff JH. Hydrogels for musculoskeletal tissue engineering. Polymers for Regenerative Medicine. Berlin, Heidelberg: Springer; 2006. p. 95–144.

[13] Muddapur UM, Alshehri S, Ghoneim MM, Mahnashi MH, Alshahrani MA, Khan AA, et al. Plant-based synthesis of gold nanoparticles and theranostic applications: A review. Molecules. 2022;27(4):1391.

[14] Rehm BH. Bacterial polymers: Biosynthesis, modifications and applications. Nat Rev Microbiol. 2010;8(8):578–92. doi: 10.1038/nrmicro2354.

[15] Rehm BH, Valla S. Bacterial alginates: Biosynthesis and applications. Appl Microbiol Biotechnol. 1999;52(3):289–97. doi: 10.1007/s002530051523.

[16] Dreaden EC, Alkilany AM, Huang X, Murphy CJ, El-Sayed MA. The golden age: gold nanoparticles for biomedicine. Chem Soc Rev. 2012;41(7):2740–79.

[17] Huang X, El-Sayed IH, Qian W, El-Sayed MA. Cancer cell imaging and photothermal therapy in the near-infrared region by using gold nanorods. J Am Chem Soc. 2006;128(6):2115–20.

[18] Dykman L, Khlebtsov N. Gold nanoparticles in biomedical applications: recent advances and perspectives. Chem Soc Rev. 2012;41(6):2256–82.

[19] Elbehiry A, Al-Dubaib M, Marzouk E, Moussa I. Antibacterial effects and resistance induction of silver and gold nanoparticles against *Staphylococcus aureus*-induced mastitis and the potential toxicity in rats. Microbiol Open. 2019;8(4):e00698.

[20] Li X, Robinson SM, Gupta A, Saha K, Jiang Z, Moyano DF, et al. Functional gold nanoparticles as potent antimicrobial agents against multi-drug-resistant bacteria. ACS Nano. 2014;8(10):10682–6.

[21] Hanora A, Ghorab M, El-Batal AI, Mosalam FA. Synthesis and characterization of gold nanoparticles and their anticancer activity using gamma radiation. J Chem Pharm Res. 2016;8(3):405–23.

[22] Kumari V, Vishwas S, Kumar R, Kakoty V, Khursheed R, Babu MR, et al. An overview of biomedical applications for gold nanoparticles against lung cancer. J Drug Deliv Sci Technol. 2023;47:777–80.

[23] Patil T, Gambhir R, Vibhute A, Tiwari AP. Gold nanoparticles: Synthesis methods, functionalization and biological applications. J Clust Sci. 2023;34(2):705–25.

[24] Bansal SA, Kumar V, Karimi J, Singh AP, Kumar S. Role of gold nanoparticles in advanced biomedical applications. Nanoscale Adv. 2020;2(9):3764–87.

[25] Keshavarz M, Moloudi K, Paydar R, Abed Z, Beik J, Ghaznavi H, et al. Alginate hydrogel co-loaded with cisplatin and gold nanoparticles for computed tomography image-guided chemotherapy. J Biomater Appl. 2018;33(2):161–9.

[26] Mirrahimi M, Khateri M, Beik J, Ghoreishi FS, Dezfuli AS, Ghaznavi H, et al. Enhancement of chemoradiation by co-incorporation of gold nanoparticles and cisplatin into alginate hydrogel. J Biomed Mater Res Part B: Appl Biomater. 2019;107(8):2658–63.

[27] Abdel-Hamid MS, Saad MW, Badawy GA, Hamza HA, Haroun AA. Synthesis and Examination of Hydroxyapatite Nanocomposites Based on Alginate Extracted from *Azotobacter chroococcum* new strain MWGH ShKB *in vitro*. Biosci Res. 2018;15(4):3293–306.

[28] Hegazi NA, Niemela SA. Note on the estimation of azotobacter density by membrane filter technique. J Appl Bacteriol. 1976;41:311.

[29] Bindhu MR, Umadevi M. Antibacterial activities of green synthesized gold nanoparticles. Mater Lett. 2014;120:122–5. doi: 10.1016/j.matlet.2014.01.108.

[30] Londonkar R, Kesralikar M. Phytochemical and in vitro anticancer activities of methanolic extract of stachytarpheta mutabilis. Acta Sci Microbiol. 2022;5(11):85–94.

[31] Haiss W, Thanh NT, Aveyard J, Fernig DG. Determination of size and concentration of gold nanoparticles from UV–Vis spectra. Anal Chem. 2007;79(11):4215–21.

[32] Tahir K, Nazir S, Li B, Khan AU, Khan ZUH, Gong PY, et al. Nerium oleander leaves extract mediated synthesis of gold nanoparticles and its antioxidant activity. Mater Lett. 2015;156:198–201.

[33] Thirumurugan A, Jiflin GJ, Rajagomathi G, Tomy NA, Ramachandran S, Jaiganesh R. Biotechnological synthesis of gold nanoparticles of *Azadirachta indica* leaf extract. Int J Biol Technol. 2010;1(1):75–7.

[34] Andrade LR, Salgado LT, Farina M, Pereira MS, Mourao PA, Amado Filho GM. Ultrastructure of acidic polysaccharides from the cell walls of brown algae. J Struct Biol. 2004;145(3):216–25.
[35] Davidson IW, Sutherland IW, Lawson CJ. Localization of *O*-acetyl groups of bacterial alginate. Microbiology. 1977;98(2):603–6.
[36] Terauchi M, Nagasato C, Inoue A, Ito T, Motomura T. Distribution of alginate and cellulose and regulatory role of calcium in the cell wall of the brown alga *Ectocarpus siliculosus* (Ectocarpales, Phaeophyceae). Planta. 2016;244:361–77.
[37] Ahumada-Manuel CL, Martínez-Ortiz IC, Hsueh BY, Guzmán J, Waters CM, Zamorano-Sánchez D, et al. Increased c-di-GMP levels lead to the production of alginates of high molecular mass in *Azotobacter vinelandii*. J Bacteriol. 2020;202(24):e00134-20.
[38] Hamouda RA, Alharbi AA, Al-Tuwaijri MM, Makharita RR. The antibacterial activities and characterizations of biosynthesized zinc oxide nanoparticles, and their coated with alginate derived from *Fucus vesiculosus*. Polymers. 2023;15:2335. doi: 10.3390/polym15102335.
[39] Madni A, Ekwal M, Ahmad S, Din I, Hussain Z, Muhammad Ranjha N, et al. FTIR drug-polymer interactions studies of perindopril erbumine. J Chem Soc Pak. 2014;36(6):064–1070.
[40] Terpáková E, Kidalová L, Eštoková A, Čigášová J, Števulová N. Chemical modification of hemp shives and their characterization. Procedia Eng. 2012;42:931–41.
[41] Movasaghi Z, Rehman S, Rehman I. Fourier Transform Infrared (FTIR) Spectroscopy of Biological Tissues. Appl Spectrosc Rev. 2008;43(2):134–79.
[42] Rath P, Bovee-Geurts PH, DeGrip WJ, Rothschild KJ. Photoactivation of rhodopsin involves alterations in cysteine side chains: detection of an SH band in the meta I– > meta II FTIR difference spectrum. Biophys J. 1994;66(6):2085–91.
[43] Anthony SE, Tisdale RT, Disselkamp RS, Tolbert MA, Wilson JC. FTIR studies of low temperature sulfuric acid aerosols. Geophys Res Lett. 1995;22(9):1105–8.
[44] Umamaheswari S, Murali M. FTIR spectroscopic study of fungal degradation of poly (ethylene terephthalate) and polystyrene foam. Chem Eng. 2013;64(19):159.
[45] Spiller N, Bjornsson R, DeBeer S, Neese F. Carbon monoxide binding to the iron–molybdenum cofactor of nitrogenase: a detailed quantum mechanics/molecular mechanics investigation. Inorg Chem. 2021;60(23):18031–47.
[46] Bouramdane Y, Fellak S, El Mansouri F, Boukir A. Impact of natural degradation on the aged lignocellulose fibers of Moroccan cedar softwood: Structural elucidation by infrared spectroscopy (ATR-FTIR) and X-ray diffraction (XRD). Fermentation. 2022;8(12):698.
[47] Periyat P, Laffir F, Tofail SAM, Magner EA. Facile aqueous sol–gel method for high surface area nanocrystalline CeO_2. RSC Adv. 2011;1(9):1794–8.
[48] Gupta BS, Jelle BP, Gao T. Application of ATR-FTIR spectroscopy to compare the cell materials of wood decay fungi with wood mould fungi. Int J Spectrosc. 2015;2014:1–8. doi: 10.1155/2015/521938.
[49] Kim BJ, Kang KS. Fabrication of a crack-free large area photonic crystal with colloidal silica spheres modified with vinyltriethoxysilane. Cryst Growth Des. 2012;12(8):4039–42.
[50] Haris MRHM, Kathiresan S, Mohan S. FT-IR and FT-Raman spectra and normal coordinate analysis of poly methyl methacrylate. Der Pharma Chem. 2010;2(4):316–23.
[51] Guo C, Liu H, Wang J, Chen J. Conformational structure of triblock copolymers by FT-Raman and FTIR spectroscopy. J Colloid Interface Sci. 1999;209(2):368–73.
[52] Juárez-de La Rosa BA, Quintana P, Ardisson PL, Yáñez-Limón JM, Alvarado-Gil JJ. Effects of thermal treatments on the structure of two black coral species chitinous exoskeleton. J Mater Sci. 2012;47:990–8.
[53] Siuda J, Perdoch W, Mazela B, Zborowska M. Catalyzed reaction of cellulose and lignin with methyltrimethoxysilane – FT-IR, ^{13}C NMR and 29Si NMR studies. Materials. 2019;12(12):2006.
[54] Wang Z, Huang B, Dai Y, Liu Y, Zhang X, Qin X, et al. Crystal facets controlled synthesis of graphene@TiO_2 nanocomposites by a one-pot hydrothermal process. CrystEngComm. 2012;14(5):1687–92.
[55] Surekha G, Krishnaiah KV, Ravi N, Suvarna RP. FTIR, Raman and XRD analysis of graphene oxide films prepared by modified hummers method. J Phys: Conf Ser. 2020;1495(1):012012.
[56] Contreras MP, Avula RY, Singh RK. Evaluation of nano zinc (ZnO) for surface enhancement of ATR–FTIR spectra of butter and spread. Food Bioprocess Technol. 2010;3:629–35.
[57] Karthikeyan V, Padmanaban A, Dhanasekaran T, Kumar SP, Gnanamoorthy G, Narayanan V. Synthesis and characterization of ZnO/NiO and its photocatalytic activity. Mechanics. Mater Sci Eng J. 2017;9:1–4.
[58] Serec K, Šegedin N, Krajačić M, Dolanski Babić S. Conformational transitions of double-stranded DNA in thin films. Appl Sci. 2021;11(5):2360.
[59] Mary YS, Ushakumari L, Harikumar B, Varghese HT, Panicker CY. FT-IR, FT-Raman and SERS spectra of L-proline. J Iran Chem Soc. 2009;6:138–44.
[60] Truică G, Teodor E, Litescu S, Radu G. LC-MS and FT-IR characterization of amber artifacts. Open Chem. 2012;10(6):1882–9.
[61] Gáplovská K, Šimonovičová A, Halko R, Okenicová L, Žemberyová M, Čerňanský S, et al. Study of the binding sites in the biomass of *Aspergillus niger* wild-type strains by FTIR spectroscopy. Chem Pap. 2018;72:2283–8.
[62] Kyriakidou M, Anastassopoulou J, Tsakiris A, Koui M, Theophanides T. FT-IR spectroscopy study in early diagnosis of skin cancer. Vivo. 2017;31(6):1131–7.
[63] Werle S, Bisorca D, Katelbach-Woźniak A, Pogrzeba M, Krzyżak J, Ratman-Kłosińska I, et al. Phytoremediation as an effective method to remove heavy metals from contaminated area–TG/FT-IR analysis results of the gasification of heavy metal contaminated energy crops. J Energy Inst. 2017;90(3):408–17.
[64] Mary YS, Raju K, Yildiz I, Temiz-Arpaci O, Nogueira HI, Granadeiro CM. Van Alsenoy C. FT-IR, FT-Raman, SERS and computational study of 5-ethylsulphonyl-2-(*o*-chlorobenzyl) benzoxazole. Colloids Surf, A. 2012;96:617–25.
[65] Jang J, Oh JH. In situ FT-IR spectroscopic investigation on the microstructure of hyperbranched aliphatic polyesters. Polymer. 1999;40(22):5985–92.
[66] Schenzel K, Fischer S. NIR FT Raman spectroscopy – a rapid analytical tool for detecting the transformation of cellulose polymorphs. Cellulose. 2001;8(1):49–57.
[67] Hadi IS, Yas RM. Gamma radiation effect on characterizations of gold nanoparticles synthesized using green method. Iraqi J Sci. 2022;2022:4305–13.
[68] Bourane A, Bianchi D. Oxidation of CO on a Pt/Al_2O_3 catalyst: from the surface elementary steps to light-off tests: IV. Kinetic study of the reduction by CO of strongly adsorbed oxygen species. J Catal. 2003;220(1):3–12.
[69] Allahbakhsh A, Sharif F, Mazinani S, Kalaee MR. Synthesis and characterization of graphene oxide in suspension and powder forms by chemical exfoliation method. Int J Nano Dimens. 2014;5(1):11–20.
[70] Ashtarinezhad A, Panahyab A, Mohamadzadehasl B, Vatanpour H, Shirazi FH. FTIR microspectroscopy reveals chemical changes in

mice fetus following phenobarbital administration. Iran J Pharm Res. 2015;14:121.
[71] Farzaneh F, Najafi M. Synthesis and characterization of Cr_2O_3 nanoparticles with triethanolamine in water under microwave irradiation. J Sci, I R Iran. 2011;22(4):329–33.
[72] Song JY, Jang HK, Kim BS. Biological synthesis of gold nanoparticles using Magnolia kobus and Diopyros kaki leaf extracts. Process Biochem. 2009;44(10):1133–8.
[73] Čempel D, Nguyen MT, Ishida Y, Tsukamoto H, Shirai H, Wang Y, et al. Au nanoparticles prepared using a coated electrode in plasma-in-liquid process: effect of the solution pH. J Nanosci Nanotechnol. 2016;16:9257–62. doi: 10.1166/jnn.2016.12923.
[74] Zhao X, Xia Y, Li Q, Ma X, Quan F, Geng C, et al. Microwave-assisted synthesis of silver nanoparticles using sodium alginate and their antibacterial activity. Colloids Surf, A. 2014;444:180–8.
[75] Watthanaphanit A, Panomsuwan G, Saito N. A novel onestep synthesis of gold nanoparticles in an alginate gel matrix by solution plasma sputtering. RSC Adv. 2014;4:1622–9.
[76] Liu H, Ikeda K, Nguyen MT, Sato S, Matsuda N, Tsukamoto H, et al. Alginate-stabilized gold nanoparticles prepared using the microwave-induced plasma-in-liquid process with long-term storage stability for potential biomedical applications. ACS Omega. 2022;7(7):6238–47.
[77] Behera M, Ram S. "Synthesis and characterization of core–shell gold nanoparticles with poly (vinyl pyrrolidone) from a new precursor salt". Appl Nanosci. 2013;3:83–7.
[78] Hinterwirth H, Wiedmer SK, Moilanen M, Lehner A, Allmaier G, Waitz T, et al. Comparative method evaluation for size and size-distribution analysis of gold nanoparticles. J Sep Sci. 2013;36(17):2952–61.
[79] Peng S, Lee Y, Wang C, Yin H, Dai S, Sun S. A facile synthesis of monodisperse Au nanoparticles and their catalysis of CO oxidation. Nano Res. 2008;1:229–34.
[80] Ahmad T, Wani IA, Lone IH, Ganguly A, Manzoor N, Ahmad A, et al. Antifungal activity of gold nanoparticles prepared by solvothermal method. Mater Res Bull. 2013;48(1):12–20.
[81] Montes MO, Mayoral A, Deepak FL, Parsons JG, Jose-Yacamán M, Peralta-Videa JR, et al. Anisotropic gold nanoparticles and gold plates biosynthesis using alfalfa extracts. J Nanopart Res. 2011;13:3113–21.
[82] Farea MO, Abdelghany AM, Oraby AH. Optical and dielectric characteristics of polyethylene oxide/sodium alginate-modified gold nanocomposites. RSC Adv. 2020;10(62):37621–30.
[83] Tajammul Hussain S, Iqbal M, Mazhar M. Size control synthesis of starch capped-gold nanoparticles. J Nanopart Res. 2009;11:1383–91.
[84] Dass A, Guo R, Tracy JB, Balasubramanian R, Douglas AD, Murray RW. Gold nanoparticles with perfluorothiolate ligands. Langmuir. 2008;24(1):310–5.
[85] Kasthuri J, Veerapandian S, Rajendiran N. Biological synthesis of silver and gold nanoparticles using apiin as reducing agent. Colloids Surf, B. 2009;68(1):55–60.
[86] Joshi P, Chakraborti S, Ramirez-Vick JE, Ansari ZA, Shanker V, Chakrabarti P, et al. The anticancer activity of chloroquine-gold nanoparticles against MCF-7 breast cancer cells. Colloids Surf, B. 2012;95:195–200.
[87] Kamala Priya MR, Iyer PR. Anticancer studies of the synthesized gold nanoparticles against MCF 7 breast cancer cell lines. Appl Nanosci. 2015;5(4):443–8.
[88] Dey S, Sherly MCD, Rekha MR, Sreenivasan K. Alginate stabilized gold nanoparticle as multidrug carrier: Evaluation of cellular interactions and hemolytic potential. Carbohydr Polym. 2016;136:71–80.
[89] Chahardoli A, Karimi N, Sadeghi F, Fattahi A. Green approach for synthesis of gold nanoparticles from *Nigella arvensis* leaf extract and evaluation of their antibacterial, antioxidant, cytotoxicity and catalytic activities. Artif Cells, Nanomed, Biotechnol. 2018;46(3):579–88.
[90] Abdelkader HS, Alhazmi NM. Disinfection of tank water using biogenic silver nanosilica as anti-microbial agents in Jeddah City. J Pharm Res Int. 2021;33(26A):14–34.
[91] Kolathupalayam Shanmugam B, Rajendran N, Arumugam K, Rangaraj S, Subramani K, Srinivasan S, et al. Curcumin loaded gold nanoparticles–chitosan/sodium alginate nanocomposite for nanotheranostic applications. J Biomater Sci, Polym Ed. 2022;34(7):875–92.
[92] Hamouda RA, Abd El Maksoud AI, Wageed M, Alotaibi AS, Elebeedy D, Khalil H, et al. Characterization and anticancer activity of biosynthesized Au/cellulose nanocomposite from *Chlorella vulgaris*. Polymers. 2021;13:3340. doi: 10.3390/polym13193340.
[93] Priya MR K, Iyer PR. Antiproliferative effects on tumor cells of the synthesized gold nanoparticles against Hep2 liver cancer cell line. Egypt Liver J. 2020;10:1–12.
[94] Otari SV, Patel SK, Jeong JH, Lee JH, Lee JK. A green chemistry approach for synthesizing thermostable antimicrobial peptide-coated gold nanoparticles immobilized in an alginate biohydrogel. RSC Adv. 2016;6(90):86808–16.
[95] Jayeoye TJ, Eze FN, Singh S, Olatunde OO, Benjakul S, Rujiralai T. Synthesis of gold nanoparticles/polyaniline boronic acid/sodium alginate aqueous nanocomposite based on chemical oxidative polymerization for biological applications. Int J Biol Macromol. 2021;179:196–205.
[96] Marsich E, Travan A, Donati I, Di Luca A, Benincasa M, Crosera M, et al. Biological response of hydrogels embedding gold nanoparticles. Colloids Surf, B. 2011;83(2):331–9.
[97] Inbaraj BS, Chen BY, Liao CW, Chen BH. Green synthesis, characterization and evaluation of catalytic and antibacterial activities of chitosan, glycol chitosan and poly(γ-glutamic acid) capped gold nanoparticles. Int J Biol Macromol. 2020;161:1484–95.
[98] Tang S, Wang Z, Li P, Li W, Li C, Wang Y, et al. Degradable and photocatalytic antibacterial Au-TiO_2/sodium alginate nanocomposite films for active food packaging. Nanomaterials. 2018;8(11):930.
[99] Hamouda RA, Qarabai FAK, Shahabuddin FS, Al-Shaikh TM, Makharita RR. Antibacterial activity of Ulva/Nanocellulose and Ulva/Ag/cellulose nanocomposites and both blended with fluoride against bacteria causing dental decay. Polymers. 2023;15:1047. doi: 10.3390/polym15041047.